Sensitivity of source localization towards conductivity anisotropy in high resolution finite element head models

A. Anwander [1], C.H. Wolters [1,2], M. Dümpelmann [3], T.R. Knösche [1]

[1]Max Planck Institute of Cognitive Neuroscience, Leipzig, Germany
[2] Max Planck Institute for Mathematics in the Sciences, Leipzig, Germany
[3] A.N.T. Software, Enschede, The Netherlands

SimBio

www.simbio.de

anwander@cns.mpg.de

www.cns.mpg.de

Introduction

In EEG/MEG source localization the human head is modeled as a volume conductor. The skull and the white matter are known to have anisotropic conductivity with a ratio of up to 1:10. Recently, formalisms have been described for relating the effective electrical conductivity tensor of white matter tissue to the effective water diffusion tensor as measured by diffusion tensor magnetic resonance imaging (DT-MRI) [1, 7]. First studies show that skull and white matter conductivity anisotropy have an influence on the forward solutions for EEG and MEG [4, 8].

This poster presents methods for creating realistically shaped high resolution finite element volume conductor models of the human head with compartments with anisotropic conductivity. Further, this study shows the influence of tissue anisotropy on the forward and inverse problem in EEG/MEG source localization.

Methods

A prerequisite for a realistic volume conductor model is the segmentation of head tissues with different conductivity properties. We used a bimodal T1-/PD-MRI approach, yielding in particular an improved segmentation of the inner skull surface [8]. Fig. 1 (left) shows an axial slice of the segmented 5-tissue head model from bimodal MRI [8].

1

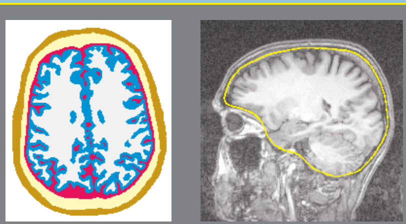

Axial slice of the 5-tissue segmentation result (left). Smooth spongiosa surface on underlying T1-MRI (right).

Generation of an anisotropic skull layer

The radial direction of the low-conducting anisotropic skull compartment is computed perpendicular to a smooth segmentation of the outer spongiosa surface using a deformable model [8] (Fig. 1, right). The skull conductivity tensor eigenvectors were generated from the radial and the two tangential directions of the surface. We used conductivity tensors $\sigma = \mathbf{S}\,\lambda\,\mathbf{S}^T$ with **S** the eigenvector matrix and simulated eigenvalues $\lambda=\mathrm{diag}(\lambda_{tang},\lambda_{tang},\lambda_{rad})$ (Table 1). λ_{rad} is the conductivity tensor eigenvalue for radial and λ_{tang} for tangential direction.

Table 1

	Skull		White matter	
Ratio	λ_{rad}	λ_{tang}	λ_{trans}	λ_{long}
1:1	0.0042	0.0042	0.14	0.14
1:2	0.0026	0.0053	0.111	0.222
1:5	0.00143	0.0072	0.0818	0.41
1:10	0.000905	0.00905	0.065	0.65

Skull and white matter conductivity tensor eigenvalue settings (in S/m). The tensor volume is kept constant for the different anisotropy ratios [8].

Generation of an anisotropic white matter layer

8 DT-MRI measurement sessions, each with 4 axially oriented, 5 mm thick slices with in-plane resolution of 2×2 mm^2 were carried out. Co-registered T1-MR images allowed the registration of the DT-MR data on the 3D T1-MR data set.

2

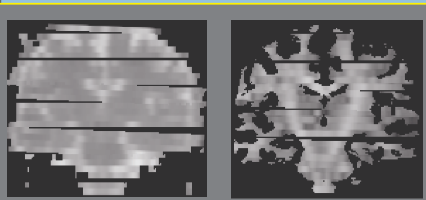

Trace of the diffusion tensor of the 8 registered DT-MRI sessions (left). Fractional anisotropy index of the DT-MRI, masked with the white matter mask of the 5-tissue segmentation result (right).

Fig. 2 (left) shows the trace of the diffusion tensors. Since water diffusion coefficients in CSF are much larger than in the brain, a large contrast is achieved at the brain surface. Fig. 2 (right) shows a map of the fractional anisotropy index of the registered DT data [8]. The highest FA value was found in the splenium of the corpus callosum (0.74). We used conductivity tensors with simulated eigenvalues $\lambda=\mathrm{diag}(\lambda_{long},\lambda_{trans},\lambda_{trans})$ (Table 1). λ_{long} is the eigenvalue longitudinal and λ_{trans} transversal to the fiber directions.

FE modeling

We generated a surface-based high resolution tetrahedral FE tessellation of the relevant 5 compartments, using CURRY [2]. Isotropic conductivity tensors were assigned to skin (0.33 S/m), CSF (1.79 S/m), brain gray matter (0.33 S/m) and ventricular system (1.79 S/m). An anisotropic conductivity tensor was assigned to each finite element in the skull and the white matter compartment (Fig. 3). Tensor validation and visualization was carried out with the SIMBIO visualization module [6].

3

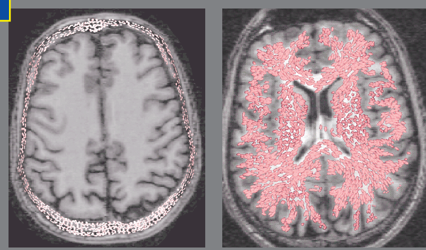

Conductivity tensors in the barycenters of skull elements (left) and white matter elements (right).

The resulting model consists of 147287 nodes and 892115 tetrahedra elements. For solving the sparse, large scale, linear FE equation system with many different right-hand-sides, we make use of our parallel NeuroFEM software [6], which is based on a parallel algebraic multigrid solver [9]. The NeuroFEM computation platform used here is an architecturally simple Linux PC-cluster with a switched Fast Ethernet connection. For inverse localization, we used a single dipole fit Nelder-Mead simplex algorithm from the SimBio inverse source localization toolbox [6, 3].

Results

4

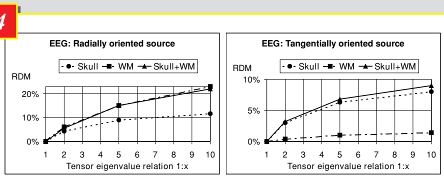

RDM errors in EEG forward result due to anisotropy with ratios from 1:1 to 1:10.

Fig. 4 shows the topographic error expressed by the relative-difference measure RDM [8], in 71 electrode EEG forward solutions for a somatosensory dipolar source in radial (left) and tangential direction (right). The errors due to anisotropy effects of skull, white matter (WM) and both skull and WM are presented. For the radial orientation, the RDM is mainly due to WM anisotropy, the error of the skull layer was only about half the one of the WM compartment. For the tangential source, the RDM is mainly due to the skull, whereas we found that WM anisotropy is negligible. For both orientations, the magnitude error, MAG [8], is close to the optimum of 1.0 (not shown).

5

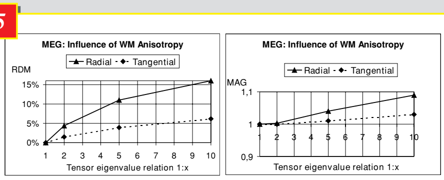

Errors in MEG forward result due to anisotropy with ratios from 1:1 to 1:10.

Fig. 5 shows RDM and MAG in MEG forward solutions for a whole head BTI 148 channel MEG system. With RDM < 1% and MAG ≈ 1, skull anisotropy was found to have no influence on the MEG (not shown). For WM anisotropy, the RDM is moderate for the tangential source, whereas it is much larger for the radial one. The MAG is again close to the optimum [8].

6

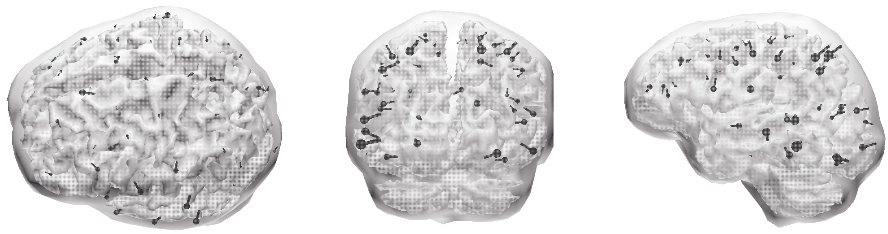

EEG localization errors due to 1:10 anisotropy of skull and WM compartment. The pole is at the position of the simulated dipole, it points to its inverse localization result. Simulated dipoles with large radial (left) and large tangential orientation component (middle and right). Errors are presented on underlying (transparent) WM and inner skull surfaces.

The influence of anisotropy to single dipole EEG source localization was computed for 43 neocortical sources with large radial (Fig. 6, left) and for 46 sources with large tangential orientation components (Fig. 6, middle and right). The EEG forward simulation in a 1:10 anisotropic (both, WM and skull) volume conductor was used as reference data for the inverse dipole fit procedure in the isotropic FE-model. For the radial sources, the largest localization error is 10.2mm, the average 5.1mm (Fig. 6, left), for the tangential it is 17.1mm and 8.8mm respectively (Fig. 6, middle and right). Tangential sources have in particular localization errors in depth. They are localized too deep in the temporal lobe (Fig. 6, middle) and too superficial in particular in parietal and occipital areas (Fig. 6, right).

Conclusion

- Our results demonstrate that skull and white matter anisotropy have a non-negligible influence on moving single dipole source localization results.
- Forward calculation and inverse localization errors indicate the necessity of the chosen complex realistic head model.
- Starting from these results, further studies will be performed to investigate other source modeling approaches, like multiple dipole source modeling, and multiple signal classification (MUSIC).

References

[1] Basser et al., Biophys. J. 66, 1994.
[2] Curry45, NeuroScan Labs, 2000.
[3] Dümpelmann et al., Biomag2002.
[4] Haueisen et al., NeuroImage, 15, 2002.
[5] Marin et al., Human Brain Mapping, 6, 1998.
[6] SimBio, http://www.simbio.de, 2000.
[7] Tuch et al., ISMRM, Sydney, 1998.
[8] Wolters et al., http://www.mpg.de/billing/, 2001.
[9] Wolters et al., Comput Visual Sci, 2002.